Self-similar coherent structures in two-dimensional decaying turbulence

1988 J. Phys. A: Math. Gen. 21 1221

(http://iopscience.iop.org/0305-4470/21/5/018)

J. Phys. A: Math. Gen. 21 (1988) 1221-1237. Printed in the UK

Self-similar coherent structures in two-dimensional decaying turbulence

R Benzi, S Patarnello and P Santangelo
IBM ECSEC, Via Giorgione 159, 00147 Rome, Italy

Received 31 July 1987

Abstract. In this paper we present a detailed study of the emergence and the long-time behaviour of coherent vortices in two-dimensional decaying turbulence. By high-resolution numerical experiments we find that the coherent structures are self-similar, i.e. their energy, enstrophy and size satisfy scaling laws. Moreover, the knowledge of the statistical distribution of the size of these vortices is sufficient to compute the energy spectrum of the 2D turbulence flow and to explain the significant deviations from the Kraichnan-Batchelor theory. At long times the motion of the fluid is dominated by the vortex dynamics, which is strikingly similar to the Hamiltonian motion of few point vortices, as is confirmed by a comparison between the numerical simulations of the two systems.

1. Introduction

In recent years many studies have been performed in order to understand the dynamical properties of two-dimensional turbulent flows. Besides purely theoretical motivations, 2D turbulence is of interest in geophysical fluid dynamics. Away from the equatorial region, large-scale oceanic and atmospheric motions can often be approximated by a quasi-two-dimensional fluid flow in a rotating frame of reference. Direct numerical integrations of 2D Navier-Stokes equations can now be performed at very high Reynolds numbers [1, 2] and some data are starting to become available from laboratory experiments [3].

In 2D fully turbulence flows one of the most interesting features, observed both in numerical and laboratory experiments, is the emergence of long-lived vortices: most of the vorticity of the turbulent flow is concentrated inside the vortices, which seem to dominate the dynamical behaviour of the system. Therefore a consistent picture of fully-developed turbulence in two dimensions requires a clear understanding of the physical properties of such coherent structures.

The emergence of vortices in these experiments poses a number of interesting questions: for instance, it is not clear whether there exists a characteristic scale for this mechanism, or whether the formation of these structures is possible even at very small scales. In other words, the relevance of initial conditions and of external forcing is not yet clear. If indeed stable vortices can exist at all scales, then substantial deviations from Batchelor-Kraichnan [4-6] theory for the initial range of the turbulent regime should be expected.

It is also necessary to provide a quantitative description about the role of the vortices in the dynamics to clarify whether these really represent the relevant part of the motion. If this is the case, only a few degrees of freedom would be necessary to

0305-4470/88/051221+17$02.50

characterise fully turbulent motion. This can have great impact on the 'predictability problem' for 2D turbulence and ultimately for its implications in geophysical flows.

In this paper some answers to the above-mentioned questions are proposed in the framework of decaying turbulence. In this case we find that coherent vortices develop at all scales of motion. As we find also that the shape of the vortices is the same at all scales, it is possible to derive a simple connection between the scale, the energy and the enstrophy for these structures. As a consequence we are able to deduce the slope of the 2D inertial range energy spectrum as a function of the number of vortices per scale (i.e. their distribution function). Coming to dynamical properties, we compare vortex trajectories obtained by high-resolution numerical integrations with those of point particles of the same vorticity in a Hamiltonian model. These two different approaches give strikingly similar results for large timescales, i.e. that large-scale properties of 2D motion can be properly described in terms of few Hamiltonian degrees of freedom.

The paper is organised as follows: § 2 describes the numerical model and some qualitative results. In § 3 we study the statistical and geometrical properties of coherent vortices. In § 4 we discuss the link between the slope of the energy spectrum and the statistical distribution of the vortices. In § 5 the comparison between the dynamics of vortices in Navier-Stokes equations and in the Hamiltonian point-like scheme is presented. Comments and conclusions are reported in § 6.

2. Description of the experiments

The Navier-Stokes equations for a 2D incompressible, purely dissipative flow are:

$$\partial_t \omega + J(\psi, \omega) = D \tag{2.1}$$

where ψ is the stream function of the system and $\omega \equiv \Delta\psi$ is its vorticity. The Jacobian ($J(a, b) = \partial_x a\, \partial_y b - \partial_x b\, \partial_y a$) and the right-hand side term D represent non-linear terms and dissipative effects respectively. As has been discussed in the introduction, we are interested in the statistical and dynamical properties of coherent structures in fully developed 2D turbulence. Therefore a set of high-resolution numerical integrations of (2.1) have been performed (512×512 degrees of freedom). In the following we point out some technical details of these numerical experiments [7].

The computational domain which we choose is a square one, with periodic boundary conditions. The linear size of this domain is 2π. The integration method consists of a de-aliased pseudo-spectral code [8]. For the dissipation term in (2.1) a superviscosity scheme is used [9], namely a term of the form $-\nu_p(-\Delta)^p\omega$, and in most experiments $p = 2$. This amounts, for a fixed numerical resolution, to working with a higher effective Reynolds number, or to moving the dissipative effects to small scales.

The stream function at $t = 0$ is defined in wave space as a complex Gaussian field with zero mean and random phases. The variance of this field is such as to give an energy spectrum which is self-similar in wave space, with a power law $E(k) \sim k^{-3}$ (see [10]). The superviscosity coefficient is $\nu_2 = 2 \times 10^{-9}$ which corresponds to a dissipative timescale which is O(1) for $k \sim 150$.

Normalisation is such that the energy of the system, defined as

$$E = \frac{1}{2V} \int_V \mathrm{d}x\, \mathrm{d}y (\nabla\psi)^2 \tag{2.2}$$

where $V=(2\pi)^2$ is the total volume of the system, is 0.5 at the beginning of the computation. In the continuous limit this quantity should be conserved, and consistently our model shows a long-time decrease of less than 1%. On the other hand, the enstrophy of the system, namely

$$Z=\frac{1}{V}\int_v \mathrm{d}x\,\mathrm{d}y(\Delta\psi)^2 \tag{2.3}$$

is not conserved in the continuous limit, and decreases from $Z\sim 150$ to $Z\sim 10$ in our experiments.

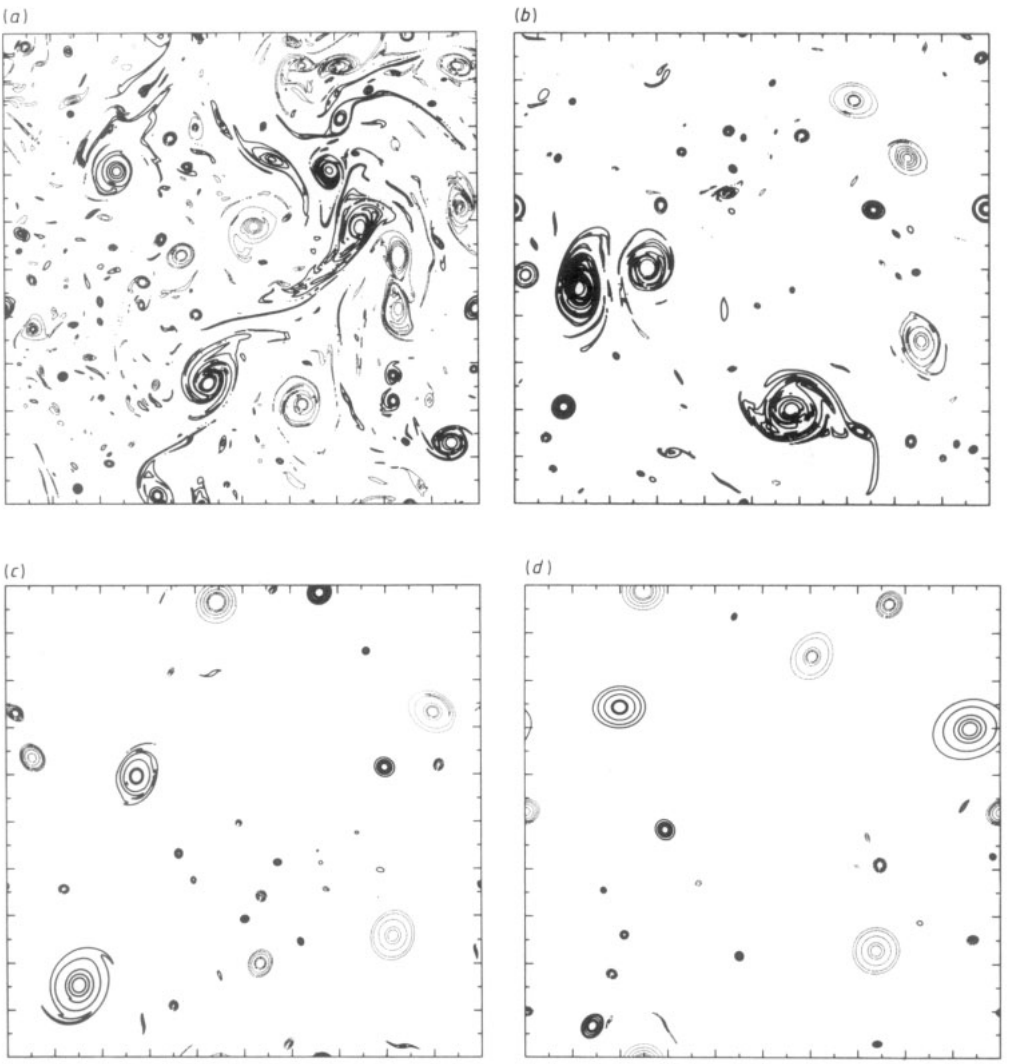

Figure 1. The vorticity field for the 512×512 experiment at $t=10$ (*a*), 20 (*b*), 30 (*c*) and 40 (*d*). The following contours are shown: 4, 8, 12, 16, 20 (full curves); −4, −8, −12, −16, −20 (dotted curves). It should be noted that after $t=30$ the number and the sizes of the coherent vortices do not change.

Numerical integrations were performed for 64 000 time steps, corresponding to 40 time units. We stress that the long duration of these runs is a peculiar feature, which has not been achieved to this extent in previous works.

The dynamical behaviour of the system can be described as follows: the short-time, transient stages are characterised by aggregation processes between patches of vorticity which, as time goes on, become anelastic collisions between well defined, coherent structures. These collisions occur between eddies of the same sign of vorticity, which therefore tend to merge to give larger stable eddies with the same shape. At long times ($t \sim 25$) the eddy dynamics seems to dominate the flow: such structures tend to stay far apart from each other and collisions no longer take place. Figures 1(a)-(d) show the time evolution of the vorticity field for the 512×512 simulation.

To interpret these results properly, one should first understand what the relevance of resolution effects is in this picture. This amounts on more physical grounds to

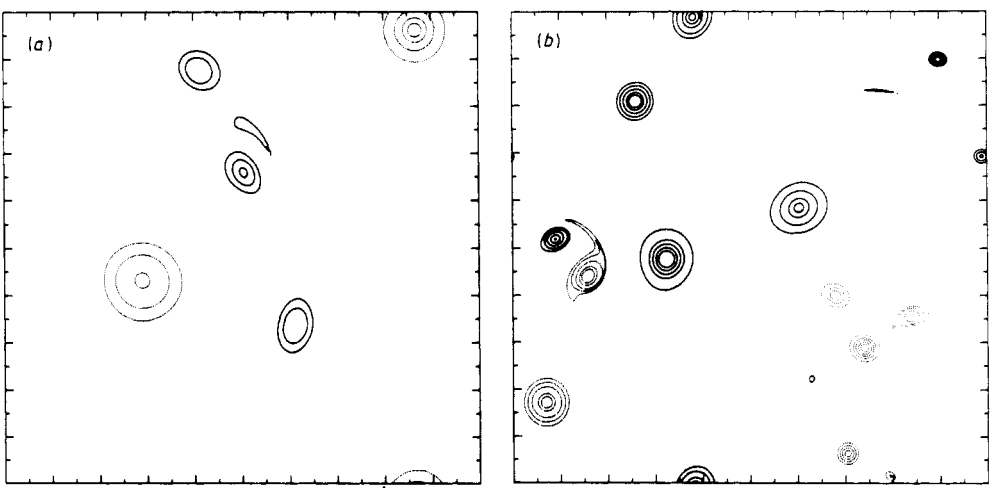

Figure 2. Same as in figure 1 for the experiment with resolution 128×128 (a) and 256×256 (b), at $t = 30$.

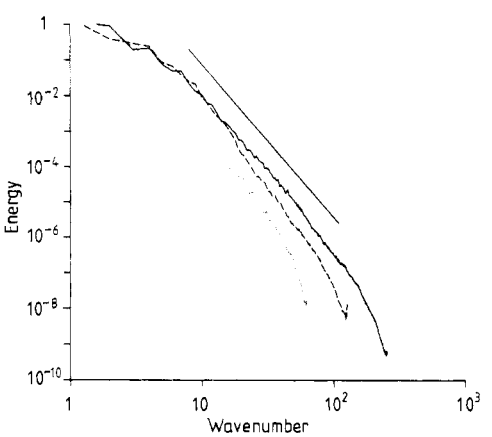

Figure 3. Energy spectra at $t = 30$ corresponding to the experiments 512×512 (full curve), 256×256 (broken curve) and 128×128 (dotted curve). The slope of the full line is -4.3.

understanding whether some kind of scaling property holds for the vortices. Figures 2(*a*), (*b*) show the vorticity field for two numerical integrations with same total initial energy ($E = 0.5$) and the same initial spectrum as in the 512×512 experiment, and resolutions 128×128, 256×256 respectively. In order to preserve physical properties at different resolutions we halve the dissipative scale when doubling the resolution scale. As a consequence, motion is more and more turbulent at a given scale when increasing resolution. From inspection of figures 1 and 2 one can state that self-similar character is preserved in the runs. That is, as resolution is increased, smaller and smaller eddies are produced. The energy spectrum $E(k)$ reflects the behaviour of the vorticity field. Figure 3 shows the energy spectra corresponding to the fields of figures 1 and 2. A well defined inertial range is shown, where $E(k) \sim k^{-4.3}$, almost independent of resolution. Moreover these spectra are definitely steeper than the one predicted by the Batchelor-Kraichnan theory of 2D turbulence, namely $E(k) \sim k^{-3}$. We will show in § 4 how the slope of the spectra is connected to the scaling properties of coherent vortices.

3. Self-similar structures of coherent vortices

We have seen at the end of the previous section that 2D decaying turbulence is characterised by the emergence of coherent vortices at every scale of length. Here we will investigate the dependence of the shape, the energy and the enstrophy of each vortex as a function of its characteristic radius.

The coherent structures shown in figure 1 can also be regarded as those regions of the fluid motion where a strong correlation holds between the vorticity field and its stream function. Indeed in figure 4 we show a scatter plot between $\psi(x, y)$ and $\omega(x, y)$ for all the points (x, y) of the square domain. For values of vorticity large in absolute value we observe a strong correlation between ω and ψ. It is worth pointing out that data plotted in figure 4 have been corrected by subtracting the advection coming from the motion of the vortex. We remark that the functional dependence of ω on ψ is non-linear. Thus a handwoven definition for a vortex consists in selecting those regions

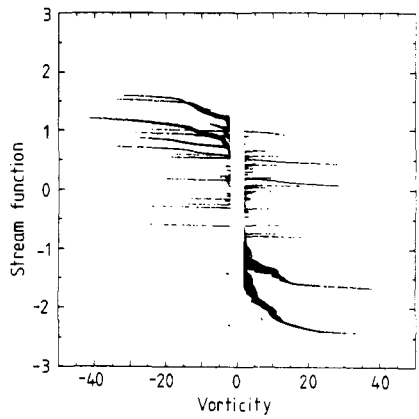

Figure 4. Scatter plot of the stream function against the vorticity for the experiment 512×512 at $r = 30$ (see figure 1(*c*)). We neglect all the points for which $|\omega| \leq 2$, to simplify the plot.

of fluid for which $|\omega(x, y)| \geq \omega_{th}$, where a suitable choice for the threshold ω_{th} is understood. The choice of this threshold is unique at all scales.

Another possible definition for a coherent vortex concerns simple criteria about the stability of the Lagrangian particles immersed in the velocity field at a given time. Given a flow configuration $\psi(x, y)$ at time t, the resulting velocity field is

$$\dot{x}_i = -\left.\frac{\partial \psi}{\partial y}\right|_{(x_i, y_i)} \qquad \dot{y}_i = \left.\frac{\partial \psi}{\partial x}\right|_{(x_i, y_i)}. \tag{3.1}$$

A small perturbation along the trajectories evolves in the following way:

$$\delta \dot{x}_i = -\left.\frac{\partial^2 \psi}{\partial y\, \partial x}\right|_{(x_i, y_i)} \delta x_i - \left.\frac{\partial^2 \psi}{\partial y^2}\right|_{(x_i, y_i)} \delta y_i \tag{3.2a}$$

$$\delta \dot{y}_i = \left.\frac{\partial^2 \psi}{\partial x^2}\right|_{(x_i, y_i)} \delta x_i + \left.\frac{\partial^2 \psi}{\partial x\, \partial y}\right|_{(x_i, y_i)} \delta y_i. \tag{3.2b}$$

The eigenvalues analysis of equations (3.2) gives

$$\lambda = \pm\sqrt{Q} \tag{3.3}$$

where

$$Q = \left(\frac{\partial^2 \psi}{\partial x\, \partial y}\right)^2 - \frac{\partial^2 \psi}{\partial^2 x}\frac{\partial^2 \psi}{\partial^2 y}. \tag{3.4}$$

From formulae (3.2) and (3.3) it follows that in the regions of the fluid where $Q < 0$ the distance between two particles embedded in the velocity field (3.1) will not diverge exponentially as a function of time. Thus one should expect that vortices are characterised by $Q < 0$. Figure 5(a) shows the contour map for Q, and figure 5(b) a one-dimensional cross section, corresponding to figure 1(c). One can notice a very good correspondence between coherent vortices and regions with $Q < 0$. We remark that the same quantity Q (which appears here having purely kinematical meaning) was used by McWilliams to claim that coherent vortices are regions of the fluid where enstrophy cascading is prevented [10].

We checked that these two definitions of coherent vortices give the same results, i.e. one can select vortices either by fixing some suitable threshold value on vorticity field or studying stability properties of Lagrangian paths. The former has the practical advantage of computational efficiency and has been used in the present analysis.

To look at scaling properties we first investigated whether a self-similar, universal character could be identified in the shape of these eddies. We conjectured a simple parametrisation of vorticity and stream function of a single vortex:

$$\omega_\nu(r) = \omega_{0\nu} f(r/R_\nu) \tag{3.5}$$

$$\psi_\nu(r) = \psi_{0\nu} g(r/R_\nu) \tag{3.6}$$

where R_ν is the radius of the vortex, and a circular symmetry for the vortex field is implied; $\omega_{0\nu}$ and $\psi_{0\nu}$ are dimensional parameters. The functions f and g have a 'universal' dependence on the quantity r/R_ν, i.e. they are independent of the specific vortex considered. These functions are connected through the equation

$$\omega(\xi) = \omega_{0\nu} f(\xi) = +\frac{\psi_{0\nu}}{R_\nu^2}\left(\frac{\mathrm{d}^2 g}{\mathrm{d}\xi^2} + \frac{1}{\xi}\frac{\mathrm{d}g}{\mathrm{d}\xi}\right) \tag{3.7}$$

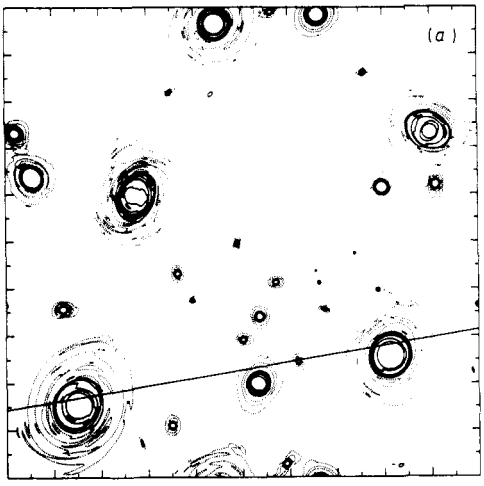

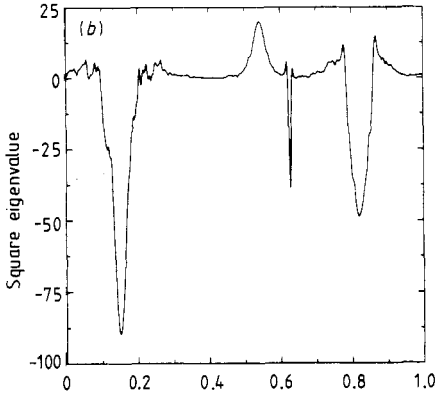

Figure 5. Contour map of Q at $t = 30$ (a). Negative values of Q (full curves) correspond to stable eigenvalues of (3.2) while positive values (dotted curves) correspond to unstable ones. Contour levels are -4, -9, -16, -25, -36 and 4, 9, 16, 25, 36. A cross section of Q along the line shown in (a) is reported in (b). Note that large instabilities occur only near the edge of the vortices.

where $\xi = r/R_\nu$. It follows that $\psi_{0\nu} = +\omega_{0\nu}R_\nu^2$. Some easy consequences from (3.5) and (3.6) can be checked. Measuring for each vortex the quantity

$$F \equiv \int_0^{R_\nu} \omega_\nu^2(x, y)\, dx\, dy \left(\int_0^{R_\nu} \omega_\nu(x, y)\, dx\, dy \right)^{-2} \tag{3.8}$$

using equation (3.5) we get

$$F = \frac{1}{2\pi R_\nu^2} \int_0^1 \xi f^2(\xi)\, d\xi \left(\int_0^1 \xi f(\xi)\, d\xi \right)^{-2}. \tag{3.9}$$

Therefore, if a unique shape characterises all vortices, plotting F for each vortex would result in a scaling law, $F \sim R^{-2}$, based on pure geometrical arguments. As a matter of fact, we report in figure 6 a plot of F against the area, for all vortices of a 512×512 numerical integration, during the time interval $\{30, 40\}$. A linear behaviour with slope -1 is clearly shown. Moreover this result does not depend on time evolution. Another

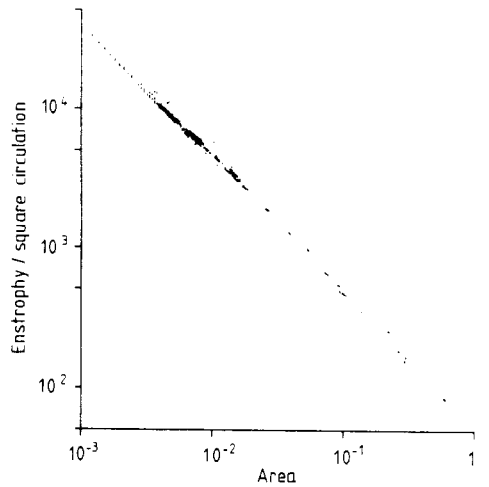

Figure 6. Plot of F against the area of each vortex in the time interval $30 \leqslant t \leqslant 40$.

check which strongly supports this universality hypothesis is the plot in figure 7, where the scatter plot of $f(\xi)$ against ξ is shown. Again a unique dependence can be recognised.

These results confirm that coherent vortices in decaying turbulence are self-similar structures. The energy and the enstrophy of each vortex are given by

$$E = C_E R_\nu^4 \omega_{0\nu}^2 \tag{3.10}$$

$$\Omega = C_\Omega R_\nu^2 \omega_{0\nu}^2 \tag{3.11}$$

where the constants C_E and C_Ω do not depend on R_ν.

From inspection of figure 1 we note that $\omega_{0\nu}$ depends very weakly on the scale of the vortex. It follows that equations (3.10) and (3.11) provide a link among the density

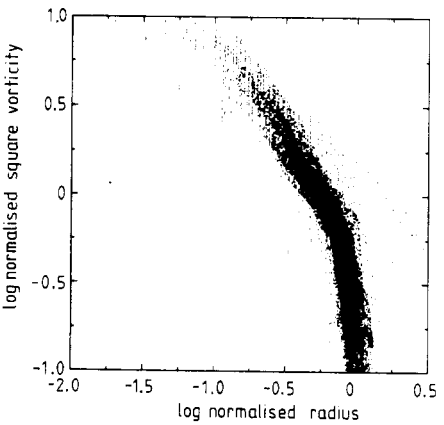

Figure 7. Scatter plot of the logarithm of the square vorticity against the logarithm of the radius at $t = 30$, for all the points inside the vortices. For each point the vorticity is normalised with the mean square vorticity of the corresponding vortex and the radius is normalised to the vortex radius, defined as the square root of the area divided by π.

distributions of vortices $\eta(R)$, i.e. the number of vortices with radius R, to the density distributions of vortex energy and enstrophy $P_1(E)$ and $P_2(\Omega)$, i.e. the number of vortices with energy E and enstrophy Ω respectively. One can easily obtain

$$P_1(E) \sim \eta(C_1 E^{1/4}) E^{-3/4} \tag{3.12}$$

$$P_2(\Omega) \sim \eta(C_2 \Omega^{1/2}) \Omega^{-1/2} \tag{3.13}$$

where C_1, C_2 are constants depending on C_E, C_Ω and $\omega_{0\nu}$. Thus the only physical quantity needed to describe scaling laws in a vortex system is $\eta(R)$. Figures 8(*a*)-(*c*) show respectively the integral distribution functions corresponding to η, P_1, P_2 as they result from our numerical integrations. All of them show a power-law behaviour,

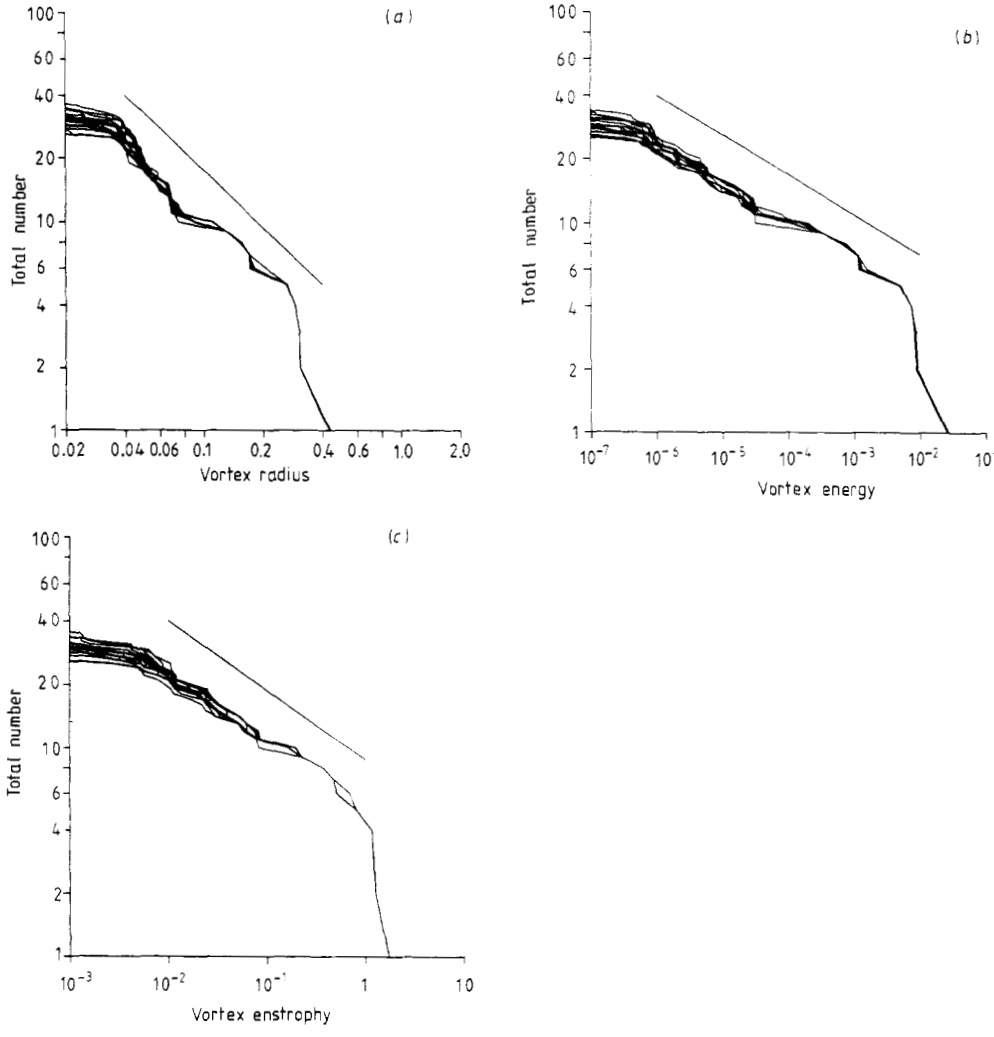

Figure 8. (*a*) Integral of the vortex radius distribution function. Many plots are superimposed for different times in the range $t = 30$-40. The slope of the full line is -0.90. Since the large vortices are more well defined, the integral is computed from right to left: $N(R_\nu) \sim \int_{R_{max}}^{R_\nu} \eta(R)\, dR$. The same integral quantities are shown for energy and enstrophy in (*b*) and (*c*) respectively and the slopes of the full lines are -0.15 and -0.33 respectively.

namely

$$\eta(R) \sim R^{-\alpha} \tag{3.14a}$$

$$P_1(E) \sim E^{-\beta} \tag{3.14b}$$

$$P_2(\Omega) \sim \Omega^{-\gamma} \tag{3.14c}$$

and the estimates of α, β and γ give

$$\alpha \sim 1.90 \tag{3.15a}$$

$$\beta \sim 1.15 \tag{3.15b}$$

$$\gamma \sim 1.33. \tag{3.15c}$$

We obtain an independent estimate for β and γ from (3.12) and (3.13). It turns out that $\beta = \frac{1}{4}(3+\alpha) = 1.22$ and $\gamma = \frac{1}{2}(1+\alpha) = 1.45$. These values are in reasonable agreement with (3.15), which once more confirms confidence in the self-similarity hypothesis. We remark that the numerical discrepancies could be connected to the weak dependence of $\omega_{0\nu}$ on R_ν.

4. The influence of coherent structures on the spectrum of the inertial range

Since Kolmogorov theory (see [4]) the energy spectrum of turbulence has been a subject of many investigations. Batchelor and Kraichnan [5, 6] (herafter referred to as BK) extended Kolmogorov theory to 2D turbulence. The major predictions of the BK theory are (*a*) that enstrophy is transferred from large to small scales and (*b*) that an inertial range proportional to k^{-3} for the energy spectra would develop in the enstrophy cascading range.

It was already observed in § 2 that such predictions have not been confirmed by some direct integrations of 2D Navier-Stokes equations [2, 10, 11]. This is also the case for our experiments. Although enstrophy is indeed transferred from large to small scales, the spectral slope of energy in the inertial range is about -4 over a wide range of wavenumbers, i.e. steeper than the BK theory predictions. To our knowledge, the only experiment which in a sense agrees with the BK theory was performed by Brachet *et al* (see [1]), where indeed a k^{-3} spectrum was observed. As a matter of fact, in that experiment no small-scale coherent structures were formed. This is very likely connected to the shape of the energy spectrum in initial conditions, which is proportional to $\exp(-k^2/k_T^2)$, where $k_T = 5$, while in our experiment the initial spectrum is near to k^{-3}. Therefore in the Brachet *et al* experiment enstrophy is initially confined at large scales, while an initial condition with k^{-3} spectrum enhances small-scale contributions. Such a difference in the initial conditions could in principle explain the different outcome of the experiments, as a different behaviour in a transient stages of the simulations. Nevertheless it would remain to understand which is the (statistically significant) asymptotic behaviour and possibly which are the characteristic times for the transient effects to be over.

To answer this question we will first show how the emergence of coherent structures can determine the spectral slope of the enstrophy cascading range. To be more specific, we will propose a connection between the scaling properties of coherent vortices (namely, their distribution function $\eta(R)$) and the energy spectrum.

Let us consider a vortex of radius R and vorticity profile

$$\omega(r) = \omega_0 f(r/R). \tag{4.1}$$

Its Fourier transform is given by

$$\Omega_R(k) = \omega_0 \int \mathrm{d}r\, \mathrm{d}\theta\, rf\left(\frac{r}{R}\right) \mathrm{e}^{-\mathrm{i}kr\cos\theta} = \frac{\omega_0}{k^2} F(kR) \tag{4.2}$$

where $F(\xi) = 2\pi \int_0^\infty \mathrm{d}x\, xf(x/\xi) J_0(x)$ and J_0 is the zeroth-order integer Bessel function. The energy spectrum for $\Omega_R(k)$ is easily obtained:

$$E_R(k) \sim \frac{|\Omega_R(k)|^2}{k} \sim \omega_0^2 k^{-5} F^2(kR). \tag{4.3}$$

Given the single-vortex contribution to the energy spectrum, we can now obtain the whole spectrum, assuming that the vorticity field outside vortices does not contribute significantly to it [12, 13]. This statement has been tested computing the energy spectrum restricted to the coherent structures, which is shown in figure 9, which agrees with the global one of figure 3 over a large range of wavenumbers.

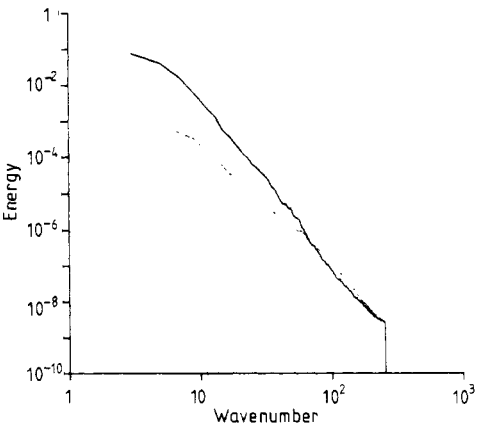

Figure 9. Energy spectrum restricted to the coherent vortices at $t = 30$ (full curve). The spectrum is almost identical to the one shown in figure 3. Coherent structures are defined as those connected regions with $|\omega| \geq 4$. The dotted curve represents the energy spectrum for the remaining part of the field. Note that the dotted spectrum is near k^{-3}.

Therefore, neglecting the vorticity field outside the coherent structures we can obtain the energy spectrum of the system by integrating (4.3) over the vortex distribution defined in § 3:

$$E(k) \sim \omega_0^2 k^{-5} \int \mathrm{d}R\, F^2(kR)\eta(R) = \omega_0^2 k^{-5} \int \mathrm{d}R\, R^{-\alpha} F^2(kR) = \omega_0^2 k^{-6+\alpha} \int \mathrm{d}\xi\, \xi^{-\alpha} F^2(\xi). \tag{4.4}$$

This computation is correct as long as the vortices do not overlap. Therefore the connection between $E(k)$ and $\eta(R)$ is established and $E(k) \sim k^{-6+\alpha}$. From the value $\alpha \sim 1.9$ previously estimated we recover $E(k) \sim k^{-4.1}$. The spectra of figures 3 and 9 have an index 4.3, in rather good agreement with this result (see also figure 10).

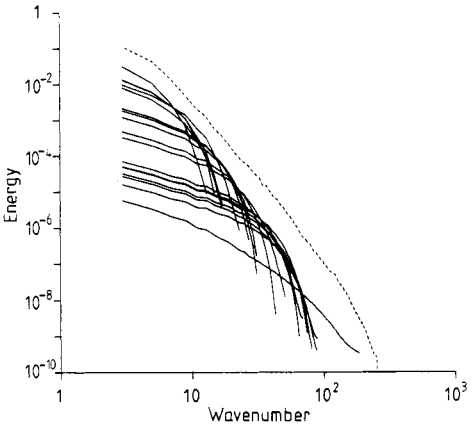

Figure 10. Energy spectra of the largest vortices (full curves) and of the total vorticity field (broken curve). The slope of the broken curve is −4.3. It is readily seen that the vortices are the dominant dynamical component; the vortices clearly determine the power-law index β of the total energy spectrum.

As is clear from this picture that the exponent α of the vortex distribution function plays a major role, it must be understood whether there exists a selection mechanism for it, which would possibly result in the definition of different universality classes, depending on the initial conditions. As we already described, in the early chaotic stages turbulence is essentially driven by aggregation processes around vorticity peaks. Thus this first phase depends strongly on initial conditions. On the other hand at later times large-scale phenomena occur as merging between eddies of the same sign and dipole-like motion of pairs of eddies. These latter events may have a universal character. Presently it is not clear to us whether the first class of processes or the second one determine the value for the index α.

In the following we propose a simple model which gives a preliminary answer to the above question. Let us consider a very large number of vortices and let R_i be the vortex radii with $R_0 \leqslant R_1 \leqslant R_2 \leqslant \ldots \leqslant R_{i-1} \leqslant R_i$. We will assume that the merging of two vortices of the same size and sign is the dominant dynamical mechanism and in particular that the merging of two vortices of radius R_k gives one vortex of radius R_{k+1}. Let n_i be the number of vortices of radius R_i. This quantity decreases due to merging in the population i and it increases due to merging in the population $i-1$. Thus we can write

$$\dot{n}_i = \frac{1}{2}\frac{n_{i-1}}{\tau_{i-1}} - \frac{n_i}{\tau_i} \tag{4.5}$$

where τ_i, τ_{i-1} are the inverse rate of merging in the population i, $i-1$ respectively. In (4.5) the factor $\frac{1}{2}$ is due to the fact that merging between two vortices of radius R_{i-1} gives one vortex of radius R_i as previously assumed. Following standard arguments of classical mechanics we can say that

$$\tau_i^{-1} = n_i \sigma_i v_i \tag{4.6}$$

where σ_i is the vortex-merging cross section and v_i the average velocity for a vortex at scale i. A rough estimate for the cross section is $\sigma_i \sim R_i$. On the other hand numerical simulations suggest that small vortices move faster than large ones (see also § 5). Thus

in a first approximation we can assume $\sigma_i v_i$ to be weakly dependent on R_i. In the following we set $\sigma_i v_i$ constant. Using (4.5) and (4.6) we obtain

$$\dot{n}_i = \tfrac{1}{2} C n_{i-1}^2 - C n_i^2. \tag{4.7}$$

On a long timescale the stationary solution of (4.7) satisfies

$$n_i = 2^{-1/2} n_{i-1} \tag{4.8}$$

which has the iterative solution

$$n_i = (\tfrac{1}{2})^{i/2} n_0 \tag{4.9}$$

where n_0 is the number of vortices with the smallest radius R_0. To get the number of vortices with given radius we assume that

$$R_i = \gamma^i R_0. \tag{4.10}$$

Equation (4.10) implies that the merging mechanism is independent of the vortex radius and all other parameters. We remark that if energy is conserved and enstrophy is dissipated during a merging then $\gamma = 2^{1/4}$. On the other hand if enstrophy is conserved and energy is produced then $\gamma = 2^{1/2}$.

By (4.9) and (4.10) we finally obtain:

$$n_i = n_0 (R_i / R_0)^{-(\ln 2)/(2 \ln \gamma)} \tag{4.11}$$

so that $\alpha = (\ln 2)/(2 \ln \gamma)$, i.e. $\alpha = 2$ for energy-conserved merging and $\alpha = 1$ for enstrophy-conserved merging. As previously observed, $\alpha \sim 1.9$ in our numerical experiments, i.e. quite close to the scheme in which energy is conserved. As a matter of fact, energy conservation is almost satisfied in our numerical integrations.

Due to the number of assumptions in our simplified model, specifically (4.7) and (4.10), it is quite surprising that equation (4.11) gives essentially the right answer. It is evident that more realistic hypotheses can be included in the model, by saying for instance that $\sigma_i v_i$ is a function of R_i rather than a constant, but this is beyond the aims of the present work. We only want to point out that a scaling law $R^{-\alpha}$ is somehow a consequence of the facts that

(*a*) a large number of vortices exists at small scales; and

(*b*) vortex merging is the only mechanism to produce large-scale vortices.

In decaying turbulence, these two requirements can be verified or not, depending on the initial conditions. More precisely, if initially enstrophy is confined to the large scales, as happens in the experiment of [1], small-scale vortices are produced only after a very long time, while large-scale vortices may be directly produced due to initial conditions. This point is currently under study [14].

5. Dynamical analysis of the vortex system

This section will be essentially devoted to some qualitative observations about vortex dynamics in numerical experiments, and to some detailed comparison with a simulation of point-like particle motion.

First of all one can compare the time dependence of the enstrophy and energy carried by vortices with that of the background field. We see from figure 11 that the set of all vortices does not dissipate significantly. Indeed every single vortex does not lose energy and enstrophy in the asymptotic regime. Hence, within a coherent vortex,

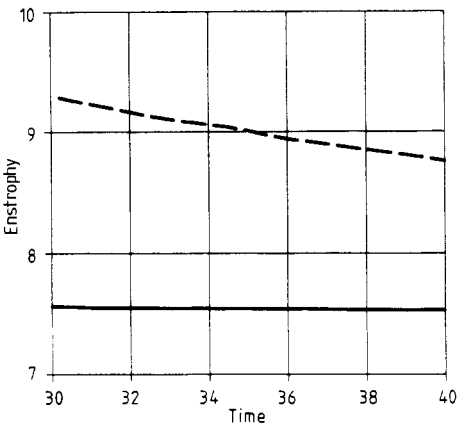

Figure 11. Enstrophy against time for the eight largest vortices (full line) and for the total system (broken line). Note the remarkable conservation of enstrophy for the vortex system.

2D turbulent flow seems to satisfy an almost inviscid equation (or at least with a dissipative timescale much longer than in the rest of the fluid).

Briefly, at least two timescales characterise the turbulent motion in a numerical simulation: one has to do with the enstrophy dissipation rate of the background field and the other with the dynamics of the vortex field and its rather slow dissipation timescale. Therefore, even though *a priori* no timescale separation can be foreseen in the 2D turbulent flow, one clearly sees that the existence of coherent structures induces a dynamical separation of timescales. This point of view is nearly opposite to the standard phenomenological theories, which predict an eddy-turnover time which is constant along the whole inertial range. These preliminary observations naturally lead to a comparison with a simple inviscid system, namely a set of point vortices following a Hamiltonian dynamics.

We start by defining the Green function $G(x, y, \bar{x}, \bar{y})$ of the Laplacian:

$$\Delta G(x, y, \bar{x}, \bar{y}) = \delta(x - \bar{x})\delta(y - \bar{y}). \tag{5.1}$$

The evaluation of G depends on the geometry of the system. Using periodic boundary conditions in our simulations, we computed G numerically in an optimised way (see for example [15]). Then the point-vortex stream function ψ can be defined as

$$\psi(x, y) = \sum_{\nu} \Gamma_\nu G_\nu(x, y, x_\nu, y_\nu) \tag{5.2}$$

where x_ν, y_ν is the position of the νth point-like vortex, and Γ_ν its vorticity strength. The time evolution of the position vector (x_ν, y_ν) is given by

$$\Gamma_\nu \dot{x}_\nu = +\frac{\partial H}{\partial y_\nu}\bigg|_{(x,y)} \tag{5.3a}$$

$$\Gamma_\nu \dot{y}_\nu = -\frac{\partial H}{\partial x_\nu}\bigg|_{(x,y)} \tag{5.3b}$$

where $H = -\Sigma_{\nu>\mu=1}^{N} \Gamma_\mu \Gamma_\nu G(x_\nu, y_\nu, x_\mu, y_\mu)$ and the self-interaction of every vortex is subtracted. As our aim is to compare this dynamics with the one given by integration of Navier-Stokes equations, we took the vortex configuration from one of the 512×512

experiment at $t = 30$ as the initial state of the pointwise system. We replaced a vortex whose centre is in (x_ν, y_ν) with a particle in the same position with a 'charge' equal to the total, integrated vorticity of the spread vortex.

Results of Hamiltonian dynamics for ten time units (figure 12) are compared with the same result obtained with the spectral code for the Navier–Stokes equation in the same time interval. Such time intervals are of the order of ten time units, whereas the instability times estimated measuring Q (see figure 5(b)) are roughly 0.2: trajectories tend to agree for times long enough for some vortices to cross the whole system. The agreement between the two instances is striking, particularly for the main, large-scale features. We remark that such a comparison is done between a system with more than 10^5 degrees of freedom (wavevectors in the Fourier decomposition) against a system with less than 20 point vortices!

The Hamiltonian equations (5.3) allow us to discuss the dynamical influence of small-scale vortices on large-scale ones. Let us consider the vortex configuration at a given time, described by the set of coordinates $\{x_\nu(t), y_\nu(t)\}$. The stability of this configuration can be determined by an eigenvalue analysis of the linearised version of (5.3), namely

$$\Gamma_\nu \delta\dot{x}_\nu = \sum_{j\neq\nu}^{N} \frac{\partial^2 H}{\partial x\,\partial y}\bigg|_j \delta x_j + \sum_{j\neq\nu}^{N} \frac{\partial^2 H}{\partial^2 x}\bigg|_j \delta y_j \tag{5.4a}$$

$$\Gamma_\nu \delta\dot{y}_\nu = -\sum_{j\neq\nu}^{N} \frac{\partial^2 H}{\partial^2 y}\bigg|_j \delta x_j - \sum_{j\neq\nu}^{N} \frac{\partial^2 H}{\partial x\,\partial y}\bigg|_j \delta y_j \tag{5.4b}$$

which holds for $\nu = 1, 2, \ldots, N$. Let λ_M be the largest eigenvalue of (5.4). This is a function of the configuration $\{x_\nu(t), y_\nu(t)\}$. Hence we can compute λ_M for each

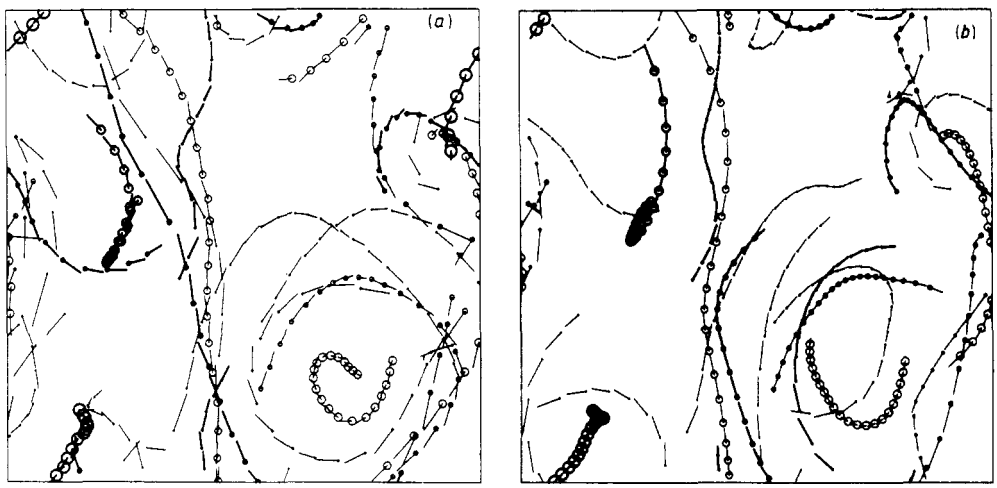

Figure 12. (a) Trajectories of the centres of the 17 largest vortices (vortex area >0.01); the plot has been obtained from the 512 × 512 simulation with the aid of a vortex recognition algorithm. The time interval plotted is 30–40. Thick (thin) lines are used for positive (negative) vortices. Circle sizes are proportional to vortex radii and segment lengths are proportional to velocities. (b) As in (a) bur for the 17 point vortices, each one having the same total vorticity Γ_ν of the corresponding vortex of the high-resolution simulation. The plot has been obtained from the solution of equations (5.3) starting with the positions of the centres of the corresponding vortices of figure 1(c). Note the striking correspondence of the trajectories of (a) and (b).

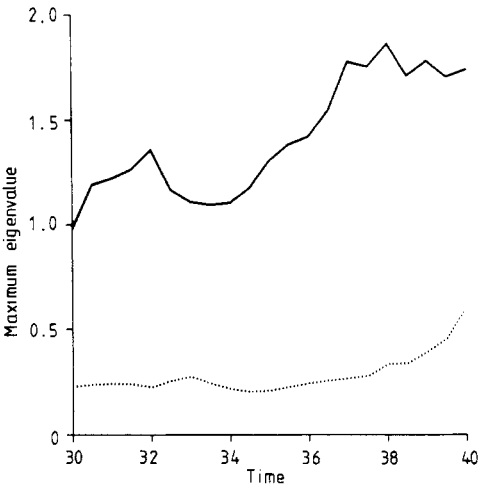

Figure 13. Plot of the largest eigenvalue (full curve) of (5.4) as a function of time for the trajectories shown in figure 12(*b*). The dotted curve represents the largest eigenvalue for the Hamiltonian system restricted to the five largest vortices.

configuration obtained integrating (5.1). The plot of $\lambda_M(t)$ is shown in figure 13. We see that λ_M is of order 1, which means that the characteristic 'predictability' time for the Hamiltonian system (5.1) is roughly 1 time unit. Comparing figures 12 and 13 we can argue that λ_M is associated to small-scale vortices. As a matter of fact, trajectories of large-scale vortices are very stable for long timescales, much larger than 1 time unit.

An interesting insight into the 'predictability' timescale of large-scale vortices can be obtained through an eigenvalue analysis similar to (5.4), but restricted on the five largest vortices. In figure 13 the quantity $\lambda_M(t)$ for this reduced system is plotted. We see that it is $\lambda_M \sim 0.2$. This implies that the predictability time for the large-scale vortices is approximately 5, i.e. larger than the characteristic time of the whole Hamiltonian system (5.3) and more than one order of magnitude larger than the Lagrangian instability timescales.

In summary we say that a 'hierarchy' of instability times exist in the system. The smallest timescales are associated to the background sea which is weakly coupled to the coherent vortices. For the latter, which are very like a Hamiltonian system, predictability times increase significantly with respect to the background sea (more than an order of magnitude). Moreover, large-scale vortices are more predictable than small-scale ones.

One may wonder whether the background vorticity field has any effect on the coherent structures. Probably the motion of coherent vortices is somehow perturbed by the effect of such background field. We can speculate that, as characteristic times of low and high vorticity fields are different, the net effect of background field on vortex motion would amount to some small random perturbation whose statistical properties are those of the low-vorticity regions.

6. Conclusions and final remarks

Due to the number of problems touched in this work, it is convenient to summarise the main results.

(i) Increasing the Reynolds number the number of vortices increases with smaller and smaller characteristic scale.

(ii) Vortices appear as approximately circularly symmetric structures, with a unique profile; the main parameter which characterises them is their radius.

(iii) The inertial range of the energy spectrum is definitely steeper than k^{-3}. Indeed the shape of the spectrum is dominated by the coherent vortices. More precisely, the energy spectrum is the superposition of the energy spectra of the single vortices.

(iv) Given these ingredients, the energy spectrum can be analytically obtained from the quantity $\eta(R)$, i.e. the distribution of the vortices with their radius R. Results of numerical simulations strongly support this point.

(v) A vortex is essentially a non-dissipative structure; i.e. enstrophy and energy of every single eddy is conserved in the asymptotic state of the motion. Even more remarkable is the fact that the long-time dynamics of such coherent structures resembles very much that of point vortices satisfying a Hamiltonian formulation. The characteristic timescale of the Hamiltonian system is much longer than that of the background field. Therefore the system itself produces a dynamical timescale separation.

This kind of analysis has strengthened the point that the 'true' collective variables for 2D turbulence are the vortices. Moreover, evidence has been provided about the existence of a dynamical separation of scales, which indeed suggests that we are faced with a problem of coupling between slow and fast variables (or, if one wishes, between Hamiltonian and Lagrangian dynamics); thus possibly some kind of clever averaging procedure appears to be a feasible strategy for this problem.

References

[1] Brachet M E, Meneguzzi M and Sulem P L 1986 *Phys. Rev. Lett.* **57** 683
[2] Benzi R, Patarnello S and Santangelo P 1987 *Europhys. Lett.* **3** 811
[3] Sommeria J and Verron J 1984 *Phys. Fluids* **27** 1918
[4] Kolmogorov A N 1941 *C.R. Acad. Sci. URSS* **30** 301
[5] Batchelor G K 1969 *Phys. Fluids Suppl. 2* **12** 233
[6] Kraichnan R H 1967 *Phys. Fluids* **10** 1417
[7] Santangelo P, Benzi R and Patarnello S 1986 *IBM ECSEC Tech. Rep.* G513-4086 p 1
[8] Patterson G S Jr and Orszag S A 1971 *Phys. Fluids* **14** 2538
[9] Basdevant R and Sadourny R 1983 *J. Mécan. Théor. Appl. Special Issue* p 243
[10] McWilliams J C 1984 *J. Fluid Mech.* **146** 21
[11] Basdevant C, Legras B, Sadourny R and Beland M 1981 *J. Atmos. Sci.* **38** 2305
[12] Babiano A, Basdevant C, Legras B and Sadourny R 1987 *J. Fluid. Mech.* in press
[13] Benzi R, Paladin G, Paternello S, Santangelo P and Vulpiani A 1986 *J. Phys. A: Math. Gen.* **19** 3771
[14] Santangelo P, Benzi R and Legras B 1987 in preparation
[15] Benzi R and Legras B 1987 *J. Phys. A: Math. Gen.* **20** 5125